J. Fluid Mech. (1984), *vol.* 145, *pp.* 447–469
Printed in Great Britain

A nonlinear stability analysis of the Bénard–Marangoni problem

By A. CLOOT AND G. LEBON
Department of Mechanics, University of Liège, B5, Sart Tilman, 4000 Liège, Belgium

(Received 20 June 1983 and in revised form 13 April 1984)

A nonlinear analysis of Bénard–Marangoni convection in a horizontal fluid layer of infinite extent is proposed. The nonlinear equations describing the fields of temperature and velocity are solved by using the Gorkov–Malkus–Veronis technique, which consists of developing the steady solution in terms of a small parameter measuring the deviation from the marginal state. This work generalizes an earlier paper by Schlüter, Lortz & Busse wherein only buoyancy-driven instabilities were handled. In the present work both buoyancy and temperature-dependent surface-tension effects are considered. The band of allowed steady states of convection near the onset of convection is determined as a function of the Marangoni number and the wavenumber. The influence of various dimensionless quantities like Rayleigh, Prandtl and Biot numbers is examined. Supercritical as well as subcritical zones of instability are displayed. It is found that hexagons are allowable flow patterns.

1. Introduction

It is a well-known fact that the onset of convection in Bénard's (1900) experiments is produced not simply by buoyancy forces but primarily by variations of the surface tension with the temperature. The latter effect is generally referred to in the literature under the name of thermocapillary or Marangoni instability. It was confirmed by Block's (1956) experimental and Pearson's (1958) analytical studies. In Pearson's theoretical model, gravity effects are ignored. Pearson's work was complemented by Nield (1964), Scriven & Sternling (1964) and Lebon & Perez-Garcia (1978), who included both mechanisms of instability. All of these analyses assumed infinitesimal small-amplitude disturbances and were unable to predict the form of the horizontal planform and the amplitude of the convective motion.

The role of the finite-amplitude perturbations can be handled within global energy methods *à la* Serrin–Joseph (Serrin 1959; Joseph 1966). This has been achieved among others by Davis (1969), Davis & Homsy (1980), Lebon & Perez-Garcia (1978) and Lebon & Cloot (1982). But, as in the case of the linear approach, the shape and the size of the cells observed beyond the critical point remain still undetermined.

Gaining information about the geometry of the convective cells requires a nonlinear analysis. The first nonlinear theory of Marangoni's problem is that of Scanlon & Segel (1967). Their model, however, is very rough: the layer is assumed to be infinitely deep, the Rayleigh number is zero and the Prandtl number is infinite. Scanlon & Segel use a successive approximation technique based on Stuart's (1960) method and predict the emergence of stable hexagonal cells at the onset of convection. Another nonlinear approach is due to Kraska & Sani (1979), whose results were not very convincing (Rosenblat, Davis & Homsy 1982). To our knowledge, the only other nonlinear analysis is that proposed recently by Rosenblat *et al.* (1982). These authors study

Marangoni convection in cylindrical and rectangular containers of finite extent. Their technique consists of expanding the field variables in series of eigenfunctions of the linear stability problem with time-dependent amplitudes. They conclude that hexagonal cells cannot appear in small-sized containers. It must, however, be observed that these results have been reached under some simplifying restrictions like a zero Rayleigh number, a zero Biot number and the no-slip condition replaced by a zero tangential vorticity along the sidewall boundaries.

In the present work, a different nonlinear approach is proposed. A layer of infinite extent is considered and our aim is to derive the three-dimensional steady solutions governing the problem near the onset of convection. Emphasis is placed on the interaction between buoyancy and surface-tension effects. The Biot number as well as the Prandtl number may take non-zero and finite values. We differ also from Rosenblat *et al.* in the technique utilized to solve the nonlinear field equations. The present analysis is carried out by using a successive approximation scheme suggested independently by Gorkov (1957) and Malkus & Veronis (1958). This technique has been applied with success by Schlüter, Lortz & Busse (1965) to the Rayleigh–Bénard problem, without surface-tension effects.

We restrict our considerations to weakly nonlinear interactions: in particular, nonlinear effects beyond the second-order approximation are omitted. Other simplifying assumptions are also introduced: the Boussinesq approximation is applied, the top free surface of the fluid is flat and non-deformable, non-inertial effects, like rotation, are omitted.

The basic equations and the Gorkov–Malkus–Veronis method are summarized in §2. The linearized problem provides the first step in any stability theory and is recalled in §3. Steady solutions to the nonlinear problem are derived in §4, where second-order approximations are obtained. However, it turns out that there still remain an infinite number of steady solutions. In order to distinguish which of them are physically preferred, we examine their stability with respect to disturbances of infinitesimal size. The stability analysis is presented in §5, where disturbances are assumed to be of the same nature as the steady solutions. Since experimental observations indicate that the latter are either rolls or hexagons, we have restricted our analysis to these two kinds of planform. In §6 we study the stability of the basic solutions with respect to perturbations of different nature, i.e. rolls with respect to hexagons and *vice versa*. The stability proof is completed in §7 by considering disturbances with wavenumbers different from the wavenumber of the reference solution. The numerical results are presented and discussed in §8, while a comparison with other theoretical models and experimental observations can be found in §9.

2. The basic equations and the Gorkov–Malkus–Veronis method

The system analysed is a horizontal viscous fluid layer, of thickness d, infinite in lateral extent, bounded on the bottom by a flat solid surface and on the top by an ambient gas. The upper free surface is assumed to remain flat and undeformable. This appears to be a reasonable hypothesis because shape deformations play a negligible role in convective instabilities as confirmed by several analyses (e.g. Smith 1966; Kraska & Sani 1979; Davis & Homsy 1980). The fluid is either heated from below or cooled at the upper surface by evaporation. In the basic state, the fluid is at rest with a steady temperature drop ΔT between the bottom and top surfaces. A Cartesian coordinate system with horizontal axes located in the lower plane and a vertical axis pointing upwards is introduced. The spatial coordinates x, y, z, the time t, the velocity

$\boldsymbol{u}(u, v, w)$ and the temperature are non-dimensionalized by dividing them by d, d^2/χ, χ/d and ΔT respectively, where χ is the thermal diffusivity of the fluid. Within the Boussinesq approximation, the velocity field $\boldsymbol{u}(u, v, w)$ and the temperature deviation θ from the linear quiescent state satisfy the relations (Scanlon & Segel 1967)

$$P^{-1}[\partial_t \nabla^2 w - \partial_{xz}(\boldsymbol{u}\cdot\boldsymbol{\nabla} u) - \partial_{yz}(\boldsymbol{u}\cdot\boldsymbol{\nabla} v) + \nabla_1^2(\boldsymbol{u}\cdot\boldsymbol{\nabla} u)] = Ra\nabla_1^2\theta + \nabla^4 w, \tag{2.1}$$

$$\partial_t(\nabla_1^2 u + \partial_{xz} w) = -P\nabla^2(\partial_y \Omega) + \partial_{xy}(\boldsymbol{u}\cdot\boldsymbol{\nabla} v) - \partial_{yy}(\boldsymbol{u}\cdot\boldsymbol{\nabla} u), \tag{2.2}$$

$$\partial_t(\nabla_1^2 v + \partial_{yz} w) = P\nabla^2(\partial_x \Omega) - \partial_{xx}(\boldsymbol{u}\cdot\boldsymbol{\nabla} v) + \partial_{xy}(\boldsymbol{u}\cdot\boldsymbol{\nabla} u), \tag{2.3}$$

$$\partial_t\theta + \boldsymbol{u}\cdot\boldsymbol{\nabla}\theta = w + \nabla^2\theta, \tag{2.4}$$

where

$$\boldsymbol{\nabla} = (\partial_x, \partial_y, \partial_z), \quad \nabla_1^2 = \partial_{xx} + \partial_{yy}, \quad \nabla^2 = \nabla_1^2 + \partial_{zz}, \quad \Omega = \partial_x v - \partial_y u;$$

Ω is the vertical component of the vorticity, subscripts t, x, y, z denote partial derivation with respect to the corresponding variables, P and Ra are the Prandtl and Rayleigh numbers, defined respectively by

$$P = \frac{\nu}{\chi}, \quad Ra = \frac{\alpha g \Delta T d^3}{\nu\chi},$$

where α is the coefficient of thermal expansion, g the acceleration due to gravity and ν the kinematic viscosity.

The relevant boundary conditions are: at the solid bottom surface $z = 0$

$$\boldsymbol{u} = 0, \qquad \theta = 0, \tag{2.5), (2.6}$$

while at the upper free surface $z = 1$

$$w = \partial_{zz} w - Ma\nabla_1^2\theta = 0, \qquad \partial_z\theta + h\theta = 0. \tag{2.7), (2.8}$$

Relations (2.5) and (2.6) express that at the bottom there is no slip and that the surface is a perfect heat conductor. Expressions (2.7) are the boundary conditions for a flat surface subject to a temperature-dependent surface tension, Ma is the Marangoni number, given by

$$Ma = -\frac{(\partial\xi/\partial T)\Delta T d}{\rho\nu\chi}, \tag{2.9}$$

where ξ is the surface tension, generally a decreasing function of the temperature, and ρ the density. Finally, (2.8) represents the thermal boundary condition at the free surface, h is the Biot heat-transfer coefficient in the fluid near the surface.

The limiting cases $h = 0$ and $h = \infty$ describe respectively an adiabatically insulated and a perfectly heat-conducting surface.

Our objective is to determine the steady solutions of the eigenvalue problem set up by (2.1)–(2.8) in the immediate vicinity of the marginal Marangoni number $M^{(0)}$ corresponding to the onset of convection. This task is achieved by expanding the field quantities $(\boldsymbol{u}, \theta)$ and the Marangoni number in powers of a small parameter ϵ:

$$\boldsymbol{u} = \sum_{i=1}^{N} \epsilon^i \boldsymbol{u}^{(i)}, \quad \theta = \sum_{i=1}^{N} \epsilon^i \theta^{(i)}, \quad Ma = M^{(0)} + \sum_{i=1}^{N} \epsilon^i M^{(i)}. \tag{2.10}$$

Substituting (2.10) in (2.1)–(2.8) and equating the different powers of ϵ yields a hierarchy of inhomogeneous differential equations. It is shown in the following sections that ϵ remains very small ($10^{-7} < \epsilon < 10^{-1}$), so that it is reasonable to restrict

the analysis to the second order of approximation. A detailed discussion of the validity of this approximation is found in §8.

As mentioned in §1, the preferred form of convection is determined by examining the stability of the steady solutions with respect to disturbances of infinitesimal size, denoted by $\tilde{\boldsymbol{u}}$ and $\tilde{\theta}$. Without loss of generality, we can express their time-dependence as

$$(\tilde{\boldsymbol{u}}, \tilde{\theta}) \sim \exp(\sigma t).$$

Although the problem is not self-adjoint, it was proved by Vidal & Acrivos (1966) that the principle of exchange of stability still holds. When the expansions (2.10) are inserted in the linearized perturbed equations, one obtains terms that are proportional to the various powers of ϵ. As stated by Schlüter *et al.* (1966), this suggests that $\tilde{\boldsymbol{u}}$, $\tilde{\theta}$ and σ be developed similarly in power series of ϵ. At each order of approximation the domain of stability of the steady solution is obtained by requiring that the real part of σ is negative; this yields the range of amplitudes ϵ for which the analysis applies.

3. The linear problem

The momentum and heat equations of the linear steady problem follow directly from (2.1)–(2.4), while the boundary conditions are given by (2.5)–(2.8) with a superscript (1) on each field variable. Their solutions are of the form

$$(w^{(1)}, \theta^{(1)}) = [W^{(1)}(z), \Theta^{(1)}(z)]\,\phi(x, y), \tag{3.1}$$

where $\phi(x, y)$ satisfies the relation (Chandrasekhar 1961)

$$\nabla_1^2 \phi + k^2 \phi = 0, \tag{3.2}$$

with $\boldsymbol{k}$ the horizontal wavenumber. A solution of (3.2) is provided by (Schlüter *et al.* 1966; Busse 1978)

$$\phi = \sum_{\substack{n=-N \\ n \neq 0}}^{N} c_n \phi_n, \quad \phi_n = \exp(\mathrm{i}\boldsymbol{k}_n \cdot \boldsymbol{r}), \tag{3.3}$$

with $|k_n|^2 = k^2$, $\boldsymbol{r}(x, y)$ is the horizontal position vector and c_n a complex quantity subject to the conditions

$$\sum_{n=-N}^{N} |c_n|^2 = 1, \quad c_{-n} = c_n^+. \tag{3.4}$$

where c_n^+ is the complex conjugate.

Solutions (3.3) corresponding to $N = 1, 2, 3$ represent two-dimensional rolls, rectangular and hexagonal cells respectively. When the notation $\mathrm{D} \equiv \mathrm{d}/\mathrm{d}z$ is used, the amplitudes $W^{(1)}$ and $\Theta^{(1)}$ obey

$$(\mathrm{D}^2 - k^2)^2 W^{(1)} = Ra\, k^2 \Theta^{(1)}, \qquad (\mathrm{D}^2 - k^2)\,\Theta^{(1)} = -W^{(1)}, \tag{3.5), (3.6}$$

with the boundary conditions

$$W^{(1)} = \mathrm{D}W^{(1)} = \Theta^{(1)} = 0 \quad \text{at} \quad z = 0, \tag{3.7}$$

$$W^{(1)} = \mathrm{D}^2 W^{(1)} + k^2 M^{(0)} \Theta^{(1)} = \mathrm{D}\Theta^{(1)} + h\Theta^{(1)} = 0 \quad \text{at} \quad z = 1. \tag{3.8}$$

This problem has been solved by Nield (1964), who used a Fourier-series expansion, and by Lebon & Perez-Garcia (1978), who employed a variational method. Neutral stability curves $M^{(0)}(k)$ corresponding to various values of Ra and h were established. The minimum value M_c of the function $M^{(0)}(k)$ represents the critical value at which convection starts.

4. The second-order approximation

The set of steady inhomogenous equations in power ϵ^2 generated by inserting (2.10) in (2.1) and (2.4) is given by

$$\nabla^4 w^{(2)} + Ra\,\nabla_1^2\theta^{(2)} = P^{-1}[\nabla_1^2(\boldsymbol{u}^{(1)}\cdot\boldsymbol{\nabla}u^{(1)}) - \partial_{xz}(\boldsymbol{u}^{(1)}\cdot\boldsymbol{\nabla}u^{(1)}) - \partial_{yz}(\boldsymbol{u}^{(1)}\cdot\boldsymbol{\nabla}v^{(1)})], \quad (4.1)$$

$$\nabla^2\theta^{(2)} + w^{(2)} = \boldsymbol{u}^{(1)}\cdot\boldsymbol{\nabla}\theta^{(1)}. \quad (4.2)$$

The equations governing the behaviour of $u^{(2)}$ and $v^{(2)}$ are of no interest at this stage. The boundary conditions keep their form (2.5)–(2.8), with superscript (2) on each variable, with the exception of (2.7*b*), which reads

$$(\partial_{zz}w^{(2)} - M^{(0)}\nabla_1^2\theta^{(2)})_1 = M^{(1)}(\nabla_1^2\theta^{(1)})_1, \quad (4.3)$$

subscript 1 means that the corresponding quantities are evaluated at the upper surface $z = 1$.

The condition of satisfying Fredholm's existence theorem leads to non-trivial solutions. The existence theorem takes a particular form because the eigenvalue $M^{(0)}$ of the homogeneous problem appears in one of the boundary conditions (Friedman 1956).

If $U = [w(x,y,z),\ \theta(x,y,z),\ \theta(x,y,z=1)]$ denotes a solution of the set (4.1)–(4.3), the solvability condition requires that the adjoint solution $\boldsymbol{U}^*$ of the linear problem be normal to the inhomogenous part of (4.1)–(4.3). Explicitly, the existence condition is

$$\frac{1}{S}\int PW^*\phi_n^+\{\sum_{m,l} c_m c_l[\nabla_1^2\boldsymbol{u}_m^{(1)}\cdot\boldsymbol{\nabla}w_l^{(1)} - \partial_{xz}(\boldsymbol{u}_m^{(1)}\cdot\boldsymbol{\nabla}u_l^{(1)}) - \partial_{yz}(\boldsymbol{u}_m^{(1)}\cdot\boldsymbol{\nabla}v_l^{(1)})]\}\,\mathrm{d}\Omega$$

$$+\frac{1}{S}\int\Theta^*\phi_n^+[\sum_{m,l} c_m c_l(\boldsymbol{u}_m^{(1)}\cdot\boldsymbol{\nabla}\theta_l^{(1)})]\,\mathrm{d}\Omega + \frac{1}{S}\int[\mathrm{D}W^*\phi_n^+ M^{(1)}\sum_m c_m\nabla_1^2\theta_m^{(1)}]_1\,\mathrm{d}S = 0$$

$$(n = -N, \ldots, N), \quad (4.4)$$

where $\mathrm{d}S$ denotes a surface element taken at $z = 1$, while

$$\boldsymbol{u}_m^{(1)} = (u_m^{(1)}, v_m^{(1)}, w_m^{(1)}) = (k^{-2}\partial_{xz}, k^{-2}\partial_{yz}, 1)\,W^{(1)}(z)\,\phi_m(x,y). \quad (4.5)$$

The adjoint problem is formulated and solved in the Appendix.

After insertion of (4.5) in (4.4), one obtains a system of $2N$ homogeneous equations for the $2N+1$ unknowns c_n and $M^{(1)}$, the $(2N+1)$th relation being provided by the normalization condition (3.4*a*). In the regular case, in which the angles between two neighbouring $\boldsymbol{k}$-vectors are always equal, all the coefficients c_n take the same value (Schlüter *et al.* 1967; Busse 1978), so that a particular solution of (4.4) is

$$c_{-N} = \ldots = c_{-1} = c_1 = \ldots = c_N = \pm(2N)^{-\frac{1}{2}}. \quad (4.6)$$

Concerning the values of $M^{(1)}$, they take different values according to whether N is equal to 1, 2 or 3.

For rolls ($N = 1$) and rectangular ($N = 2$) planforms, one finds that $M^{(1)} = 0$. For hexagonal cells $M^{(1)}$ is non-zero and given by

$$M^{(1)} = \pm\left(\frac{2}{3}\right)^{\frac{1}{2}}\frac{F(-\frac{1}{2})}{k^2(\Theta^{(1)}\,\mathrm{D}W^*)_1}, \quad (4.7)$$

where

$$F(-\tfrac{1}{2}) = \int_0^1\{P^{-1}\,W^*\tfrac{1}{2}[\mathrm{D}(W^{(1)}\,\mathrm{D}^2W^{(1)}) + \tfrac{1}{2}\mathrm{D}(\mathrm{D}W^{(1)})^2 - 3W^{(1)}\,\mathrm{D}W^{(1)}]$$

$$+\Theta^*(W^{(1)}\,\mathrm{D}\Theta^{(1)} + \tfrac{1}{2}\Theta^{(1)}\,\mathrm{D}W^{(1)})\}\,\mathrm{d}z. \quad (4.8)$$

The solutions corresponding to $N > 3$ have not been observed experimentally and therefore are not analysed in the present work.

After the solvability condition has been established, it remains to calculate the second-order solutions $w^{(2)}$ and $\theta^{(2)}$. They are of the form

$$(w^{(2)}, \theta^{(2)}) = (w_{\mathrm{H}}^{(2)}, \theta_{\mathrm{H}}^{(2)}) + (w_{\mathrm{p}}^{(2)}, \theta_{\mathrm{p}}^{(2)}), \tag{4.9}$$

where $(w_{\mathrm{H}}^{(2)}, \theta_{\mathrm{H}}^{(2)})$ are the solutions of the second-order homogeneous problem and are formally identical with the first-order solutions $w^{(1)}$ and $\theta^{(1)}$; $(w_{\mathrm{p}}^{(2)}, \theta_{\mathrm{p}}^{(2)})$ are particular solutions and are assumed to consist of two parts:

$$(w_{\mathrm{p}}^{(2)}, \theta_{\mathrm{p}}^{(2)}) = \sum_{m,l} (w_{ml}^{(2)}, \theta_{ml}^{(2)}) \phi_m \phi_l + \sum_{m} (\bar{w}_m^{(2)}, \bar{\theta}_m^{(2)}) \phi_m, \tag{4.10}$$

$(w_{ml}^{(2)}, \theta_{ml}^{(2)})$ are solutions of the non-homogeneous set (4.1), (4.2) and the homogeneous left-hand side of (4.3); $(\bar{w}_m^{(2)}, \bar{\theta}_m^{(2)})$ are solutions of the homogeneous parts of (4.1) and (4.2) and the complete equation (4.3). The second-order solutions are derived in Cloot (1983), to which the reader is referred for detailed calculations. The values of $M^{(2)}$ are obtained from the solvability conditions of the third-order solutions. Despite the restrictions imposed by the solvability conditions, we are still faced with an infinite number of steady solutions, namely the set of all regular solutions consisting of rolls, rectangular and hexagonal cells. To remove this degeneracy, we shall examine the stability of the solutions with respect to infinitesimally small perturbations.

5. Stability of the steady solutions

In the present section we restrict the analysis to small disturbances with wavenumber $\tilde{\boldsymbol{k}}$ identical with wavenumber $\boldsymbol{k}$ of the basic steady solution.

Let $\tilde{\boldsymbol{u}}(\tilde{u}, \tilde{v}, \tilde{w})$ and $\tilde{\theta}$ be the small-amplitude perturbations of the steady solution $u(u, v, w)$ and θ with a time-dependence of the form $\exp(\sigma t)$. The disturbances $\tilde{\boldsymbol{u}}$ and $\tilde{\theta}$ obey a set of equations that are readily derived by linearizing (2.1)–(2.4). The boundary conditions are still given by (2.5)–(2.8) with a tilde on every field variable. When the series expansions (2.10) for u and θ are used, one obtains equations with terms proportional to the powers of ϵ. This has motivated Schlüter *et al.* (1967) to develop similarly the growth rate σ and the disturbances $\tilde{\boldsymbol{u}}$ and $\tilde{\theta}$ in terms of the same parameter ϵ:

$$\sigma = \sigma^{(0)} + \sum_{i=1} \epsilon^i \sigma^{(i)}, \tag{5.1}$$

$$\tilde{\boldsymbol{u}} = \tilde{\boldsymbol{u}}^{(0)} + \sum_{i=1} \epsilon^i \tilde{\boldsymbol{u}}^{(i)}, \quad \tilde{\theta} = \tilde{\theta}^{(0)} + \sum_{i=1} \epsilon^i \tilde{\theta}^{(i)}. \tag{5.2}$$

The coefficients of each power of ϵ generated by inserting (5.1) and (5.2) in the equations satisfied by $\tilde{\boldsymbol{u}}$ and $\tilde{\theta}$ must vanish identically. As a result, we are faced with a sequence of linear inhomogeneous equations setting up an eigenvalue problem for the growth rates $\sigma^{(i)}$, with $i = 0, 1, 2, \ldots$. We now discuss briefly each order of approximation.

5.1. *Zeroth-order analysis*

For $i = 0$ the relevant equations are

$$\nabla^4 \tilde{w}^{(0)} + Ra \nabla_1^2 \theta^{(0)} - P\sigma^{(0)} \nabla^2 \tilde{w}^{(0)} = 0, \tag{5.3}$$

$$\nabla^2 \tilde{\theta}^{(0)} + \tilde{w}^{(0)} - \sigma^{(0)} \theta^{(0)} = 0, \tag{5.4}$$

$$\partial_{zz} \tilde{w}^{(0)} - M^{(0)} \nabla_1^2 \tilde{\theta}^{(0)} = 0 \quad \text{at} \quad z = 1, \tag{5.5}$$

which, with the exception of the last terms in (5.3) and (5.4), are the same as the equations of the linearized steady problem. As a consequence, by selecting disturbances for which $\sigma^{(0)} = 0$, which are the most unfavourable perturbations for $\tilde{\boldsymbol{k}} = \boldsymbol{k}$, the solutions $\tilde{w}^{(0)}$ and $\tilde{\theta}^{(0)}$ are of the form (3.1), with ϕ_n still given by (3.3), but with coefficients $\tilde{c}_n$ different from c_n.

5.2. *First-order analysis*

The set to be solved turns out to be

$$\nabla^4 \tilde{w}^{(1)} + Ra\,\nabla_1^2 \tilde{\theta}^{(1)} = P^{-1}[\sigma^{(1)} \nabla^2 \tilde{w}^{(0)} + N_1(\boldsymbol{u}^{(1)}, \tilde{\boldsymbol{u}}^{(0)})], \tag{5.6}$$

$$\nabla^2 \tilde{\theta}^{(1)} + \tilde{w}^{(1)} = \sigma^{(1)} \tilde{\theta}^{(0)} + \boldsymbol{u}^{(1)} \cdot \boldsymbol{\nabla} \tilde{\theta}^{(0)} + \tilde{\boldsymbol{u}}^{(0)} \cdot \boldsymbol{\nabla} \theta^{(1)}, \tag{5.7}$$

$$\partial_{zz} \tilde{w}^{(1)} - M^{(0)} \nabla_1^2 \tilde{\theta}^{(1)} = M^{(1)} \nabla^2 \tilde{\theta}^{(0)} \quad \text{at} \quad z = 1, \tag{5.8}$$

where $N_1(\boldsymbol{u}^{(1)}, \tilde{\boldsymbol{u}}^{(0)})$ is given by

$$N_1(\boldsymbol{u}^{(1)}, \tilde{\boldsymbol{u}}^{(0)}) = \nabla_1^2(\boldsymbol{u}^{(1)} \cdot \boldsymbol{\nabla} \tilde{w}^{(0)} + \tilde{\boldsymbol{u}}^{(0)} \cdot \boldsymbol{\nabla} w^{(1)}) - \partial_{xz}(\boldsymbol{u}^{(1)} \cdot \boldsymbol{\nabla} \tilde{u}^{(0)} + \tilde{\boldsymbol{u}}^{(0)} \cdot \boldsymbol{\nabla} u^{(1)}) - \partial_{yz}(\boldsymbol{u}^{(1)} \cdot \boldsymbol{\nabla} \tilde{v}^{(0)} + \tilde{\boldsymbol{u}}^{(0)} \cdot \boldsymbol{\nabla} v^{(1)}).$$

The existence theorem leads to a system of $2N$ linear homogeneous equations for the $2N$ unknowns $\tilde{c}_n$, namely

$$\tilde{c}_n(B\sigma^{(1)} - E^{(1)}) + \sum_l a\delta_{(ln)\frac{1}{3}\pi} \tilde{c}_l = 0 \quad (n = -N, \ldots, +N), \tag{5.9}$$

where

$$B = \int_0^1 [\tilde{\boldsymbol{\Theta}}^* \boldsymbol{\Theta}^{(1)} - P^{-1} \tilde{W}^* (\mathrm{D}^2 W^{(1)} - k^2 W^{(1)})]\,\mathrm{d}z, \tag{5.10}$$

$$E^{(i)} = k^2 M^{(i)} (\boldsymbol{\Theta}^{(1)} \mathrm{D} \tilde{W}^*)_i \quad (i = 1, 2, \ldots), \tag{5.11}$$

$$a = \pm \left(\frac{2}{N}\right)^{\frac{1}{2}} F(-\tfrac{1}{2}), \tag{5.12}$$

while Kronecker's symbol $\delta_{(ln)\frac{1}{3}\pi}$ is equal to 1 when the angle between $\boldsymbol{k}_l$ and $\boldsymbol{k}_n$ is 60° and zero otherwise. An upper asterisk denotes the solution of the adjoint problem at order 0. The solutions of (5.9) are non-trivial when the determinant formed by the coefficients of $\tilde{c}_n$ vanishes. This yields a relation between $\sigma^{(1)}$ and the parameters Ra, P, h, $M^{(0)}$ and $M^{(1)}$.

We shall only handle two cases of practical interest, namely $N = 1$ (rolls) and $N = 3$ (hexagons), and determine in both cases the sign of the eigenvalues $\sigma^{(1)}$. For rolls one obtains

$$\sigma_{\mathrm{RR}}^{(1)} = 0, \tag{5.13}$$

where the subscript RR means that one examines the stability of steady rolls with respect to disturbances themselves taking the form of rolls. The result (5.13) indicates that rolls are marginally stable.

Suppose now that the basic planform is constituted by hexagonal cells ($N = 3$). The vanishing of the characteristic equation leads to the result

$$\sigma_{\mathrm{HH}}^{(1)} = \frac{3a}{B}, \frac{2a}{B}, 0, -\frac{a}{B}. \tag{5.14}$$

Since at least one of the eigenvalues $\sigma_{\mathrm{HH}}^{(1)}$ is positive, it is inferred that, at the first order, hexagons are unstable.

The next step is to ensure whether this conclusion is confirmed by a higher-order analysis.

5.3. *Second-order analysis*

Repeating the above analysis up to the second order yields the values of $\sigma^{(2)}_{RR}$ and $\sigma^{(2)}_{HH}$. The values of $\sigma^{(2)}_{HH}$ are determined numerically and it is seen that there exist regions where

$$\sigma_{HH} = \epsilon\sigma^{(1)}_{HH} + \epsilon^2\sigma^{(2)}_{HH} < 0 \tag{5.15}$$

for every mode, indicating that hexagonal cells are stable at the present order of investigation.

For disturbances taking the form of rolls, the question of stability does not receive a definite answer. Indeed it turns out that

$$\sigma^{(2)}_{RR} = 0, -E^{(2)}/B. \tag{5.16}$$

Numerically, it is seen that $-E^{(2)}/B$ is always negative, so that the highest eigenvalue is $\sigma^{(2)}_{RR} = 0$. As a consequence, it can be said that, up to the second order of approximation, rolls are marginally stable with respect to the particular class of disturbances that are considered in this section. At this point of the analysis, it is not possible to predict which structure, either rolls or hexagons, is preferred. A final answer can only be obtained by including a larger class of disturbances, as will be done in §6.

6. Stability of steady solutions with respect to disturbances of different nature

6.1. *Stability of rolls versus hexagons*

In this section we consider disturbances whose coefficients $\tilde{c}_n$ may be non-zero for eigenvectors $\tilde{\boldsymbol{k}}_n$ different from the eigenvalues $\boldsymbol{k}_n$ pertaining to the steady reference solution. In the study of stability of rolls versus hexagons, one has $M^{(1)} = 0$, and the existence condition of the first-order solutions yields a set of $2N$ equations in the $2N$ unknowns $\tilde{c}_n$. Since the developments are similar to these of §5.2, we reproduce only the main results.

For a relative distribution of the perturbed $\tilde{\boldsymbol{k}}_n (n = 1, 2, \ldots, 6)$ with respect to the reference wavenumbers $\boldsymbol{k}_1, \boldsymbol{k}_2$ represented on figure 1, the vanishing of the characteristic determinant leads to

$$\sigma^{(1)}_{RH} = -a/B, 0, a/B. \tag{6.1}$$

Since two of the eigenvalues are of opposite sign, it is clear that rolls are unstable versus the above type of disturbances. In figure 1 the wavenumbers of the perturbed and the steady solutions are seen to coincide. By selecting other configurations where the $\tilde{\boldsymbol{k}}_n$ are rotated with respect to the $\boldsymbol{k}_n$, one finds that $\sigma^{(1)}_{RH}$ vanishes. However, this result cannot modify the earlier conclusion, since one single positive $\sigma^{(1)}_{RH}$ is sufficient to lead to instability.

6.2. *Stability of hexagons versus rolls*

It can be shown that

$$\sigma^{(1)}_{HR} = \sigma^{(1)}_{HH} = a/B, \tag{6.2}$$

whatever the relative orientations of the perturbed and the reference wavenumbers. The quantity a/B can be either positive or negative. Stability demands that

$$\sigma_{HR} = \epsilon\sigma^{(1)}_{HR} < 0, \tag{6.3}$$

which is satisfied if ϵ and $\sigma^{(1)}_{HR}$ are of opposite signs. This condition provides a

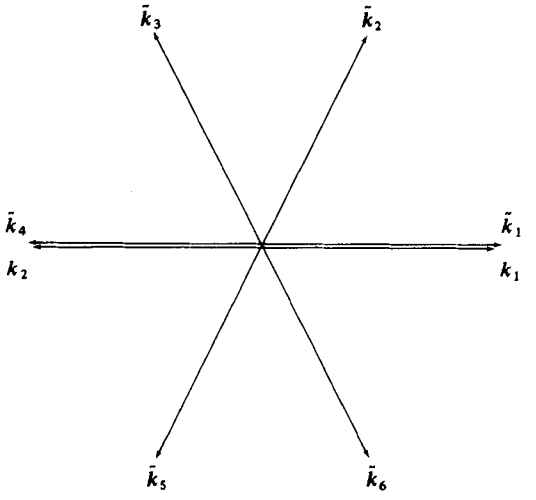

FIGURE 1. Distribution of the wavevectors $\tilde{k}$ of the disturbance with respect to the wavevectors k of the reference roll cell.

supplementary restriction, which complements the limitation placed by inequality (5.15) on the allowable values of ϵ.

To be complete, it remains to examine the stability of the steady states with respect to disturbances of the same nature as the basic solution, but with a wavenumber $\tilde{k} \neq k$.

7. Stability with respect to disturbances of wavenumbers $\tilde{k} \neq k$

Unlike the results of §§5 and 6, we are no longer entitled to identify the perturbed zero-order solutions $\tilde{w}^{(0)}, \tilde{\theta}^{(0)}$ and their adjoints $\tilde{w}^*, \tilde{\theta}^*$ with the solutions $w^{(1)}, \theta^{(1)}$ and w^*, θ^* of the linear steady problem. Moreover, $\sigma^{(0)}$ is not necessarily zero. For more details the reader is referred to the Appendix.

Let us briefly review the various orders of approximation. At the zero linearized order, the equations can be written as

$$\boldsymbol{L} \cdot \tilde{\boldsymbol{U}} = 0, \tag{7.1}$$

where $\tilde{\boldsymbol{U}} = (\tilde{w}^{(0)}, \tilde{\theta}^{(0)}, \tilde{\theta}_1^{(0)})$, while $\boldsymbol{L}$ is defined by relation (A 19) (see Appendix). The solutions of (7.1) are still of the form

$$(\tilde{w}^{(0)}, \tilde{\theta}^{(0)}) = (\tilde{W}^{(0)}(z), \tilde{\Theta}^{(0)}(z)) \sum_n \tilde{c}_n \tilde{\phi}_n, \tag{7.2}$$

with

$$\tilde{\phi}_n = \exp \mathrm{i}(\tilde{\boldsymbol{k}}_n \cdot \boldsymbol{r}), \quad |\tilde{\boldsymbol{k}}_n|^2 = \tilde{k}^2 \quad \forall n. \tag{7.3}$$

At the first order it follows from the Fredholm theorem that

$$\sigma_{\mathrm{HH}}^{(1)} = \tilde{a}/\tilde{B}, \tag{7.4}$$

where $\tilde{B}$ and $\tilde{a}$ are given respectively by (5.10) and (5.12) with a tilde on each field variable. Stability holds if

$$\sigma_{\mathrm{HH}} = \sigma_{\mathrm{HH}}^{(0)} + \epsilon \sigma_{\mathrm{HH}}^{(1)} < 0. \tag{7.5}$$

This inequality determines a new domain of allowable values of ϵ. The actual zone of stability results from the intersection of the three stability domains defined by

inequalities (5.15), (6.3) and (7.5) respectively. The numerical calculations, reported in §8, show the existence of a narrow domain of stability. The analysis has been pursued up to the second order and $\sigma_{\mathrm{HH}}^{(2)}$ has been computed; the results are commented upon in §8.

At this point of the analysis, we feel it necessary to summarize the contents of the five last sections. As a first step (§§ 3 and 4), we have determined the steady velocity and temperature fields in the close vicinity of the onset of convection. In the remaining sections (5, 6 and 7), we have studied the stability of the solutions. First, we have examined (§5) the stability with respect to infinitesimally small disturbances exhibiting the same properties (same configuration and same wavenumber) as the reference solution. We have found that rolls as well as hexagons may be stable. We have then introduced disturbances with a pattern different from that of the basic solution (§6). We have shown that rolls cannot exist because they are unstable with respect to 'hexagonal' disturbances. In contrast, hexagonal cells are stable with respect to perturbations taking the form of rolls. Finally, in §7 we have completed the proof of stability of hexagonal patterns by considering disturbances with a wavenumber different from the wavenumber of the steady solution. The results have been established for disturbances taking the form of hexagons with $\tilde{\boldsymbol{k}}$ (disturbance) $\neq \boldsymbol{k}$ (reference). The same conclusions hold for disturbed configurations consisting of rolls because expressions of $\sigma_{\mathrm{HR}}^{(1)}$ and $\sigma_{\mathrm{HR}}^{(2)}$ are similar to those of $\sigma_{\mathrm{HH}}^{(1)}$ and $\sigma_{\mathrm{HH}}^{(2)}$.

8. Results and discussion

8.1. *The numerical procedure*

The various problems handled in this note are solved by using the Davidov–Flechter–Powell minimization technique in connection with the Rayleigh–Ritz method. The latter implies that the governing differential equations are replaced by variational principles. Unfortunately, since most of the equations involved are non-self-adjoint, it is hopeless to construct 'exact' variational principles. Only so-called 'restricted' principles (Finlayson 1972; Lebon 1980) can be formulated; the governing field equations are recovered as Euler–Lagrange equations, but at the cost of freezing, during the variational procedure, some variables in the functional to be extremalized. An example of restricted variational equation is provided by

$$\delta I(W, \Theta, \overset{0}{W}, \overset{0}{\Theta}) = 0, \tag{8.1}$$

where δ is the usual variational symbol while 0 over a character indicates that the corresponding quantity is not varied. Despite their restricted character, one can use the classical variational methods, like the Rayleigh–Ritz method. The latter consists of expanding the field variables, e.g. $W(z)$ and $\Theta(z)$, in the form

$$W = \sum_{i=1}^{m} a_i f_i(z), \qquad \Theta = \sum_{i=1}^{n} b_i g_i^{(z)}, \tag{8.2), (8.3}$$

where a_i and b_i are unknown constants while $f_i(z)$ and $g_i(z)$ are *a priori* given functions selected here as

$$f_i = z^2(1-z)\,T_{i-1}^*, \qquad g_i = z(1-\tfrac{1}{2}z)\,T_{i-1}^*, \tag{8.4), (8.5}$$

which satisfies the essential boundary conditions, T_i^* are the modified Tchebyshev polynomials. The procedure is traditional and will not be detailed here. Convergence is attained with a maximum of six terms in the expansions (8.2) and (8.3).

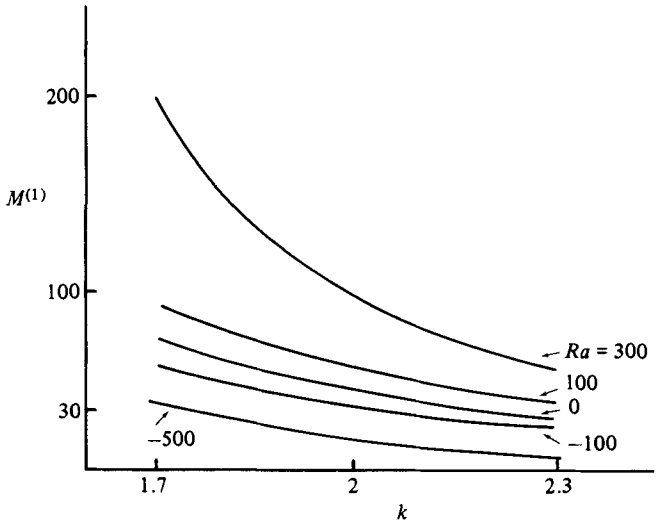

FIGURE 2. The first-order Marangoni number $M^{(1)}$ versus the wavenumber k for $P = 7$, $h = 0$ and various values of the Rayleigh number Ra.

The calculations have been performed for several values of the Rayleigh number ranging from

$$Ra = -500 \quad \text{to} \quad Ra = 669,$$

three values of the Prandtl number,

$$P = 7, 70, 500,$$

and two values of the Biot number,

$$h = 0, 1.$$

The negative values of Ra correspond to fluid layers either heated from above or heated from below, with a negative coefficient of thermal expansion. The value $Ra = 669$ is characteristic of a layer with a critical Marangoni number equal to zero (Nield 1964). The values 7 and 500 of the Prandtl number describe respectively water and a viscous oil; $P = 70$ is an intermediate value. The two values $h = 0$ and $h = 1$ of the Biot number define an adiabatically insulated and a weakly conducting upper surface respectively.

8.2. *First-order results*

The values of $M^{(0)}(k)$ have been calculated earlier (Nield 1964; Lebon & Perez 1980), so that our first objective is to determine $M^{(1)}(k)$.

Plots of $M^{(1)}(k)$ versus the wavenumber k for $h = 0$ and various values of the Rayleigh number are shown on figures 2 and 3. For Ra-values such that $-500 \leqslant Ra \leqslant 300$ (figure 2) $M^{(1)}$ decreases monotonically and changes its sign when k is increased beyond a value k_D larger than the critical value k_c predicted by the linear theory. For $400 \leqslant Ra \leqslant 669$ figure 3 shows vertical asymptotes occurring at values k_D, smaller than k_c for $Ra < 600$, and larger than k_c for Ra-values exceeding 600. The behaviour of $\sigma^{(1)}$ is similar to that of $M^{(1)}$ with change of sign and asymptotes at k_D values of the wavenumber. Clearly, our model will fail for k-values near k_D, where $M^{(1)}$ tends to infinity.

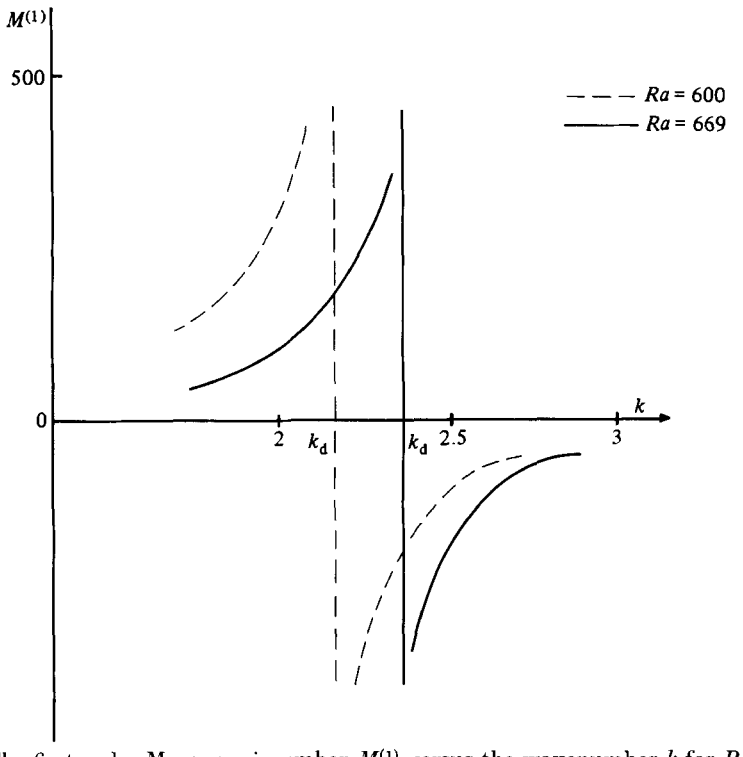

FIGURE 3. The first-order Marangoni number $M^{(1)}$ versus the wavenumber k for $P = 7$, $h = 0$ and various values of the Rayleigh number Ra.

8.3. *Second-order results* ($\tilde{\boldsymbol{k}} = \boldsymbol{k}$)

It was stated in §7 that steady rolls are unstable. Therefore our stability analysis will exclusively concern hexagonal solutions. Up to the second order in ϵ, the rate of growth of the disturbances is given by

$$\sigma_{\mathrm{HH}} = \epsilon(\sigma^{(1)}_{\mathrm{HH}} + \epsilon\sigma^{(2)}_{\mathrm{HH}}). \tag{8.6}$$

Imposing $\sigma_{\mathrm{HH}} < 0$, one finds the range of allowable values of ϵ corresponding to stability. The regions of stable convective hexagons are represented by shaded areas on figure 4.

The values of ϵ versus k, shown on figure 4, obey the condition (6.3) to be of opposite sign to $\sigma^{(1)}_{\mathrm{HR}}$, as imposed by the stability of hexagons versus rolls. The stability regions are located at one side of the asymptotes $k = k_{\mathrm{D}}$: at the left for $Ra \leqslant 500$, and at the right for $Ra \geqslant 600$. When buoyancy effects overcome surface-tension effects (which corresponds to values of $Ra \geqslant 600$), it is seen that the supercritical wavenumbers are larger than the critical wavenumber k_{c}. This remains true in the limiting case of a zero critical Marangoni number ($Ra = 669$). However, when surface effects become predominant ($Ra < 500$), the situation is reversed and the supercritical wavenumbers are smaller than k_{c}.

8.4. *Second-order results* ($\tilde{\boldsymbol{k}} \neq \boldsymbol{k}$)

Unlike the case $\tilde{\boldsymbol{k}} = \boldsymbol{k}$, the growth rate $\sigma^{(0)}$ is no longer equal to zero. A numerical study shows that the system is stable with respect to modes $\boldsymbol{k}$ satisfying

$$Ma^{\mathrm{c}}|_{\tilde{k}} > Ma^{\mathrm{c}}|_{k_{\mathrm{ref}}},$$

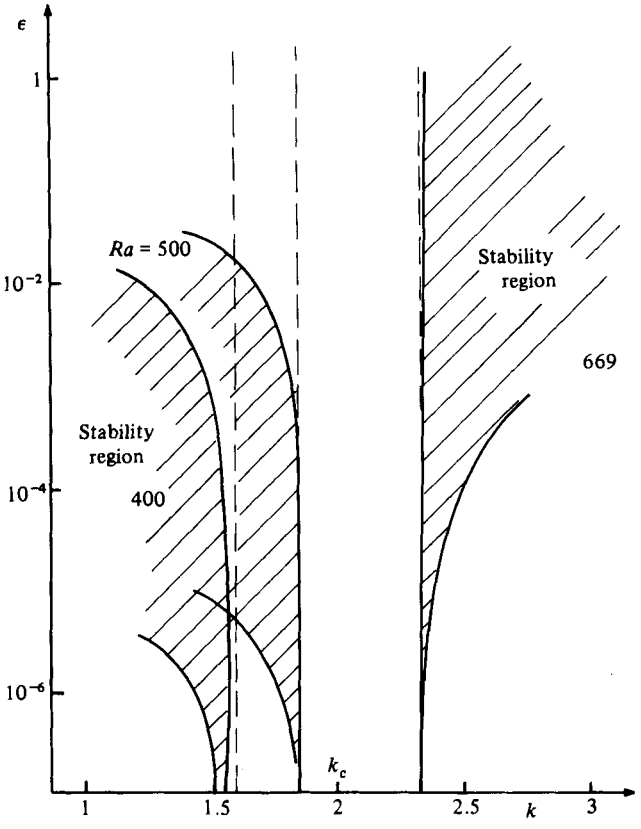

FIGURE 4. The stability regions in the (ϵ, k)-plane for $P = 7$, $h = 0$ and various values of the Rayleigh number.

because in that case $\sigma^{(0)} < 0$. Otherwise one has $\sigma^{(0)} > 0$, and a higher-order analysis is necessary. The calculations have been extended up to the second order, and the corresponding stability ranges are drawn on figure 5. Whereas the upper line $\epsilon_{\max}(k)$ is unaffected by the order of approximation, the lower curve $\epsilon_{\min}(k)$ is appreciably lowered by passing from the first to the second order. For comparison, we have also represented the curve $\epsilon_{\min}(k)$ corresponding to the case $\tilde{\boldsymbol{k}} = \boldsymbol{k}$.

8.5. *Stability domains in the* (Ma, k)*-plane*

The actual stability domain results from the intersection of three stability domains corresponding to three different classes of disturbances, namely disturbances with $\boldsymbol{k}$-vectors equal to those of the steady motion, disturbances with $\tilde{\boldsymbol{k}}$-vectors different from those of the steady motion, and disturbances with coefficients $\tilde{c}_n$ different from the c_n of the steady state.

The stability ranges in the (Ma, k)-plane are obtained by replacing, in

$$Ma = M^{(0)} + \epsilon(k)\, M^{(1)} + [\epsilon(k)]^2\, M^{(2)}, \tag{8.7}$$

the quantity $\epsilon(k)$ by its minimum and maximum allowable values respectively. Unless otherwise stated, the Prandtl and Biot numbers have been fixed equal to 7 and 0 respectively.

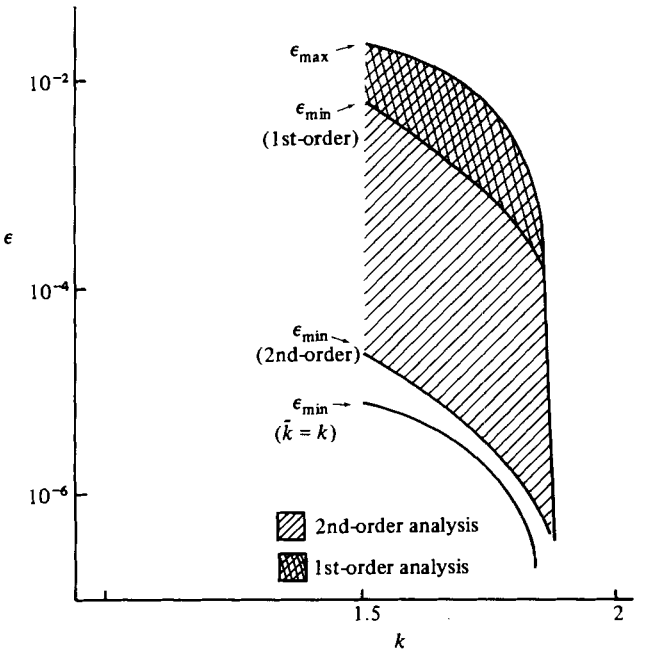

FIGURE 5. Comparison of the stability domains corresponding to the first- and second-order analyses respectively. $P = 7$, $h = 0$.

Bearing in mind that for rolls $M^{(1)} = 0$, whereas for hexagons $M^{(1)}$ is seen to be numerically negligible with respect to $M^{(2)}$, it is justifiable to write

$$\epsilon^2 = \frac{Ma - M^{(0)}}{M^{(2)}}.$$

The magnitude of $Ma^{(2)}$ (up to 10^{10}) ensures the smallness of the parameter ϵ, whose values run from 10^{-1} to 10^{-7}.

A qualitative picture of the stability range of hexagonal cells is represented on figure 6(a,b) for $Ra = 669$ and 600. The allowed states of convection are located in regions where $k > k_c$. As mentioned earlier, stable cells are found in regions where $k < k_c$ when Ra is decreased. This is illustrated on figure 7(a,b) where Ra takes the values 500 and 400. When surface effects become dominant ($Ra = 100$ and $Ra = 0$), the stability range is shifted anew to regions where $k > k_c$ (see figures 8a,b). Moreover, a new phenomenon is displayed, namely the occurrence of a subcritical instability where $Ma < M^{(0)}$, i.e. where the linear theory predicts a state of rest. Although the subcritical band is rather narrow, it enlarges with increasing k-values. The presence of a region of subcriticality has also been detected for negative Ra values.

We now fix P and Ra but allow h to vary. It is observed on figure 9 that for $Ra = 500$ and $P = 70$ the stability zones grow with h and are displaced towards smaller values of k when the Biot number is increased. Clearly, an increase of the heat exchange between the fluid layer and its environment increases the sizes of the convective cells.

The influence of Prandtl number is displayed in figure 10. By increasing P one reduces the extent of the stability domain. A similar behaviour was predicted by Busse (1978) for a layer with an upper stress-free surface in the range of intermediate and large Prandtl numbers. This effect can be tentatively interpreted by recalling that an increase of P reinforces viscous dissipation and consequently the stability of the basic quiescent state. Therefore, in order to get and maintain convection, greater

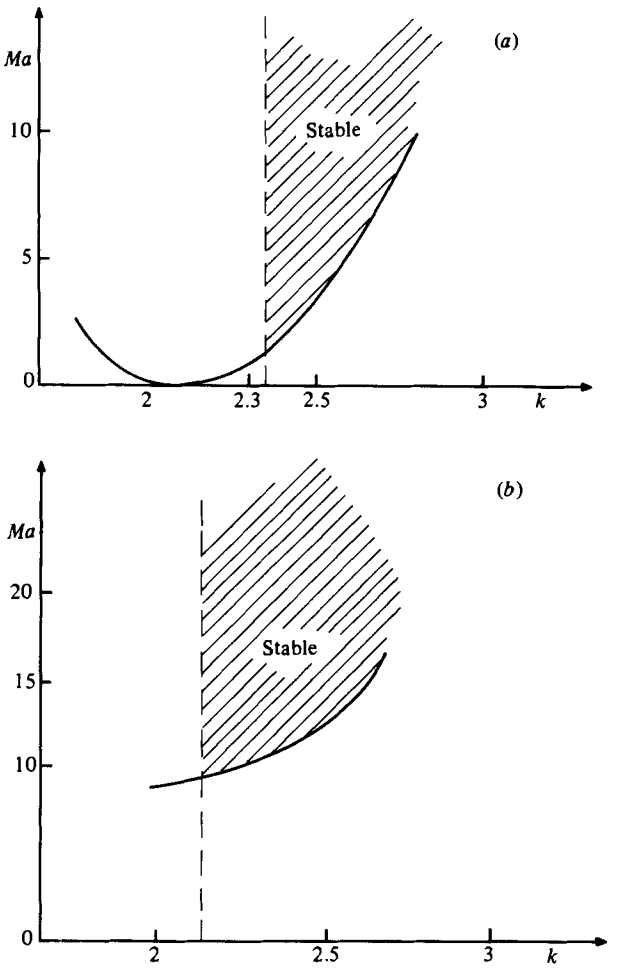

FIGURE 6. Domain of stable convective hexagons for $P = 7$, $h = 0$, $Ra = 669$ (a) and $Ra = 600$ (b). The lower curve is the marginal stability curve $M^0(k)$.

values of the velocity are required to balance the thermoviscous damping. Since high-velocity fields are more sensitive to disturbances, one can reasonably expect that the area of stability is the smallest for the largest P.

Before closing this discussion, we wish to make two additional comments. Although it is implicitly assured that ϵ is non-zero, one observes that the stability domains are confined below by the neutral stability curves $M^{(0)}(k)$. Certainly, $\epsilon_{\min}(k)$ does not vanish, but is generally so small that it cannot be represented on a picture.

It may be asked whether third- and higher-order terms in (2.10) do not alter the above conclusions. To answer this question, it is necessary to study the accuracy of the second-order approximation. This task is achieved by considering with Malkus & Veronis (1966) and Busse (1967) the convection heat transport H given by

$$H = \int_0^1 \Theta W \, \mathrm{d}z, \tag{8.8}$$

as a measure of the quality of the approximation. It is assumed that the second order of approximation is satisfactory when, by adding one term in the expansion of $H_{(2)}$, the latter differs from $H_{(3)}$ by less than 1 %. This allows us to compute the range of

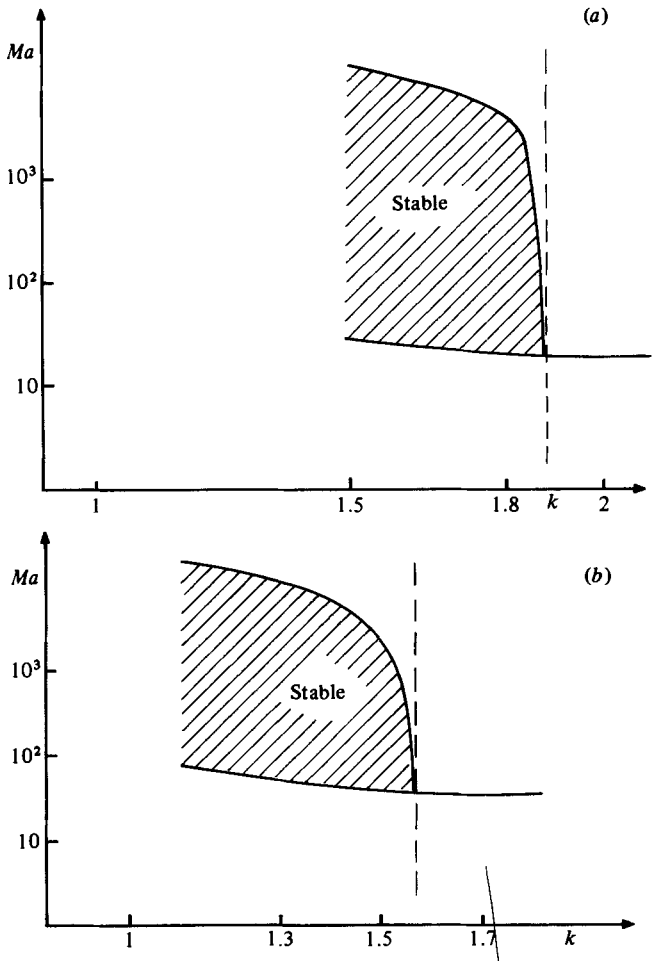

FIGURE 7. Domain of stable convective hexagons for $P = 7$, $h = 0$, $Ra = 500$ (a) and $Ra = 400$ (b). The lower curve is the marginal stability curve.

Ma-values for which a good qualitative description of the flow is expected. Substitution of (2.10) in (8.8) yields at the second and third order respectively

$$H_{(2)} = \epsilon^2 N^{(2)}, \quad H_{(3)} = \epsilon^2 N^{(2)} + \epsilon^3 N^{(3)}, \tag{8.9}$$

with

$$N^{(2)} = \int_0^1 \Theta^{(1)} W^{(1)} \, \mathrm{d}z, \quad N^{(3)} = \int_0^1 (\Theta^{(1)} W^{(2)} + \Theta^{(2)} W^{(1)}) \, \mathrm{d}z. \tag{8.10}$$

The values of $N^{(2)}$, $N^{(3)}$ and ϵ for $h = 0$ and different values of Ra, P and k are presented in table 1. We have also reported the range of Ma-values corresponding to a relative error $(H_{(3)} - H_{(2)})/H_{(2)}$ less than 1%. The results indicate that the supercritical range may extend to Ma-values considerably above the critical value. This finds its origin in the large values of $Ma^{(2)}$. Moreover, it is worth mentioning that large Ma-values are not anomalous, and are typical of fluid layers with a common thickness and a reasonable temperature drop, as confirmed by table 2, where all the values correspond to $Ra = 500$.

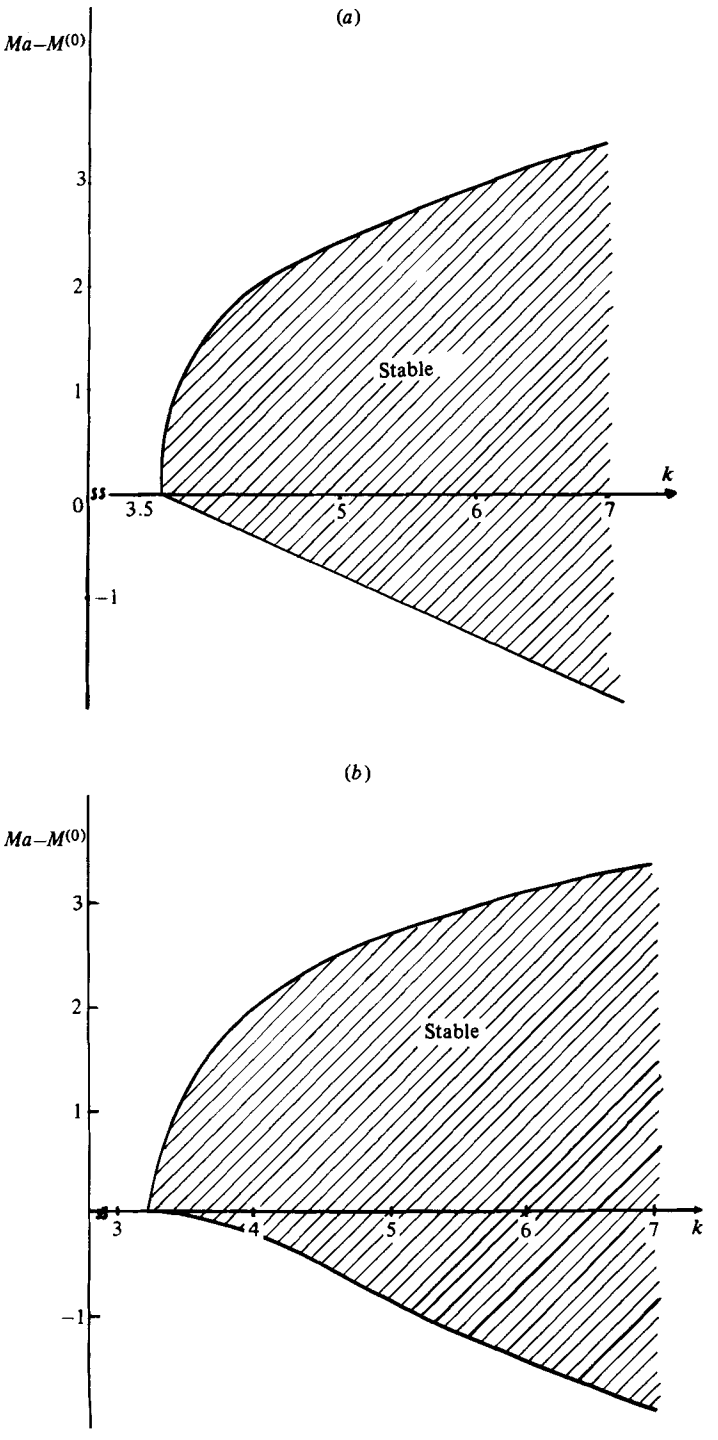

FIGURE 8. Domain of stable convective hexagons for $P = 7$, $h = 0$, $Ra = 100$ (*a*) and $Ra = 0$ (*b*). A region of subcritical instability is displayed.

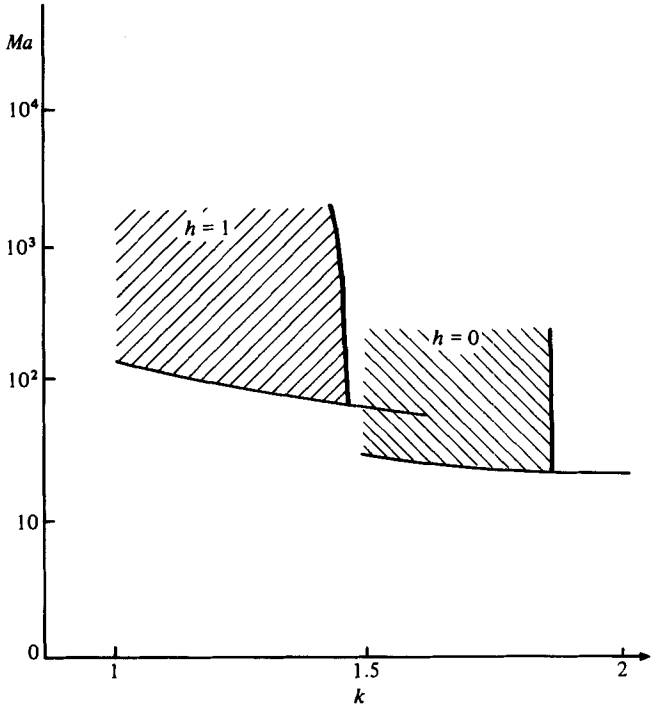

FIGURE 9. Influence of the Biot number on the extent on the stability domain in the (Ma, k)-plane for $P = 70$, $Ra = 500$.

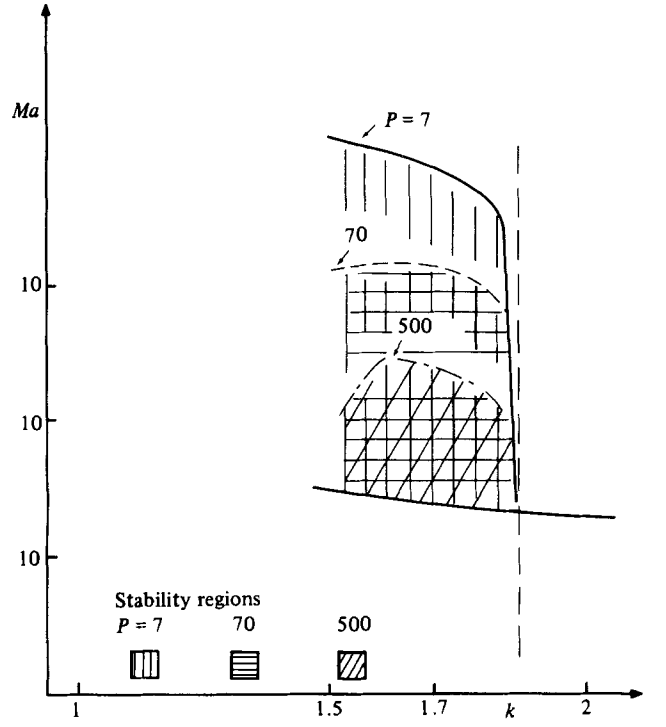

FIGURE 10. Influence of the Prandtl number on the extent of the stability domain in the (Ma, k)-plane for $Ra = 500$ and $h = 0$.

Ra	P	k	$N^{(2)}$	$N^{(3)}$	ϵ	ΔMa
0	7	4.5	4.5×10^{-3}	5.9×10^{-5}	0.15	168.9–171.5
100	7	4.5	5×10^{-3}	3.6×10^{-5}	0.15	160.2–162.8
400	7	1.3	107.5	−61.2	8.7×10^{-3}	51–9250
500	7	1.6	32.9	−31.8	1.87×10^{-2}	27–3000
500	70	1.6	32.9	−23.8	1.38×10^{-2}	27–152
500	500	1.6	32.9	−24	1.37×10^{-2}	27–44
600	7	2.6	1.89	−0.385	4.9×10^{-2}	15–523
669	7	2.6	4	−1.14	3.5×10^{-2}	5.5–264

TABLE 1. Heat-transport coefficients and Ma-range corresponding to an error less than 1 %

P	Ma	h	$\Delta T(°)$	d (cm)
7 (water)	5×10^3	0	0.8	0.4
	10^4	0	2.27	0.3
	3×10^4	1	8	0.2
500 (silicone oil)	350	0	5	0.4

TABLE 2. Characteristic Ma-values

	Scanlon & Segel ($P=\infty$)	Rosenblat *et al.* $P=0.1$	Rosenblat *et al.* $P=\infty$	Present work $P=7$
$\frac{Ma-M_a^c}{M_a^c}$	2.3 %	0.18 %	1.4 %	0.3 % ($k=4$)

TABLE 3. Extent of the subcritical domain ($Ra=0$)

9. Comparison with other work, and final comments

Of course, it is desirable to compare our predictions with other theoretical results and experimental observations. Unfortunately, reliable results exist only in two limiting cases, namely $Ma=0$, $Ra\neq0$ and $Ra=0$, $Ma\neq0$.

As mentioned earlier, Scanlon & Segel (1967) were the first to propose a nonlinear approach to Marangoni's problem. Using a very crude model, they found stable hexagonal cells within a rather wide supercritical region and a small subcritical band. The existence of a region of subcritical instability has recently been confirmed by Rosenblat *et al.* (1982), who examined nonlinear Marangoni convection in side-bounded layers. Their results together with these of Scanlon and Segel are compared with our own results in table 3.

It appears that the three analyses are in satisfactory agreement. Unlike the case $Ma\neq0$, $Ra=0$, the case $Ma=0$, $Ra\neq0$ has been treated in numerous papers. Of particular interest to us is the work of Schlüter *et al.* (1965), because, like them, we use the Gorkov–Malkus–Veronis iterative procedure. Schlüter *et al.* consider a fluid layer of infinite horizontal extent, confined either between two rigid surfaces, two free surfaces, or a rigid and a free surface; moreover each face is supposed to be perfectly heat-conducting ($h=\infty$). It is shown that rolls are the only stable configuration, with a supercritical wavenumber greater than k_c.

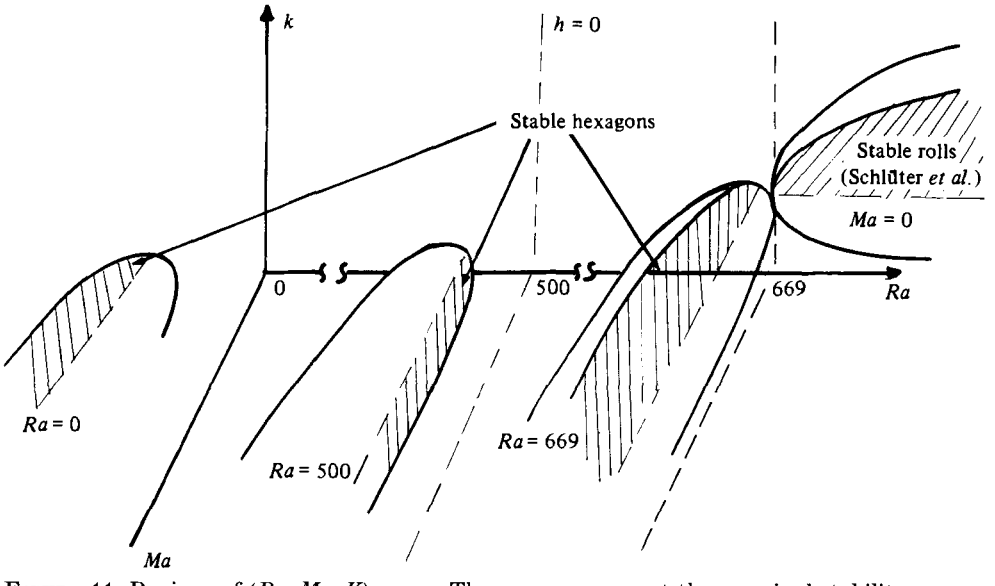

FIGURE 11. Regions of (Ra, Ma, K)-space. The curves represent the marginal stability curves obtained by projection either into the (Ma, k)-plane or into the (Ra, k)-plane.

In the present analysis it is concluded that hexagons are the preferred convection patterns, while rolls are unstable. This is by no means in contradiction with the results of Schlüter *et al.* as illustrated on figure 11 where the stable states are represented on a three-dimensional graph (Ma, Ra, k). The thick curves are the marginal stability curves obtained by projection onto the (Ma, k)- and (Ra, k)-planes respectively. Clearly it appears that our theory covers sectors which are different from those treated by Schlüter *et al.* They examine only situations in the (Ra, k)-plane with Ma fixed and set equal to zero, while we study more particularly what happens in the (Ma, k)-planes for various values of Ra.

Concerning experimental confirmation, let us first mention Block's (1956) observation that in a fluid layer heated from above – to which corresponds a negative Rayleigh number – the motion sets up in the form of hexagonal cells, in agreement with our predictions. In order to make comparisons with other experimental results, we have calculated the horizontal component $u_h = (u^2+v^2)^{\frac{1}{2}}$ of the velocity at the upper surface. The results for thin layers of water ($P = 7$) and silicone oil ($P = 500$) submitted to a temperature drop of 1 °C are reported in table 4 and compared with experimental values (ESA 1981): the experimental and theoretical values are of the same order of magnitude.

A problem of great concern during recent decades has been the variation of the supercritical wavenumber, i.e. the size of the convective cell, with Rayleigh number. Although most theories predict a supercritical wave number k larger than the critical value k_c (e.g. Schlüter *et al.* 1965), no stable flow with a wavenumber $k > k_c$ seems to have been observed (Koschmieder 1981). In the present analysis, both situations with $k < k_c$ and $k > k_c$ are encountered. When Ra lies in the intermediate range $100 < Ra < 400$, stable cells are characterized by wavenumber smaller than k_c. However, in the extreme regions where either the buoyancy effect ($Ma = 0$) or the surface-tension effect ($Ra = 0$) dominates, stable wavenumbers are larger than k_c. No conclusive argument explaining this behaviour can be advanced.

Water ($Ra = 0$)			Silicone oil ($Ra = 500$)		
k	u_h(theoretical) 10^{-2} m/s	u_h(experimental) 10^{-2} m/s	k	u_h(theoretical) 10^{-2} m/s	u_h(experimental) 10^{-2} m/s
3.5	16		1.5	1.6	
4.5	10	10	1.6	6.7	$00.1 < u_h < 10$
5	7.5		1.7	0.7	—
6.5	7.7		1.8	0.3	—

TABLE 4. Horizontal velocity at the upper surface

It must be realized that the present model is unable to answer some important questions raised by Marangoni instability. Our treatment is based on a perturbation technique and provides only solutions for limited ranges of Ma. The present analysis no longer permits us to distinguish the flow direction. It has been recognized (e.g. Palm 1975) that the temperature dependence of the viscosity is the essential factor in the determination of the sense of the motion. But this demands that we give up the Boussinesq approximation, which the present investigation relies upon. Moreover, we cannot provide a mechanism of selection among the set of allowable wavenumbers, as the layer is assumed of infinite extent. Finally, surface deflections have been neglected.

Despite its limitations, we venture to think that the present model will contribute to a better understanding of the Marangoni effect. It is also the hope that this work will instigate more laboratory observations.

Appendix

A.1. *The adjoint problem of the linearized basic problem*

The first-order equations may be written as

$$\mathsf{L}\boldsymbol{U} = 0, \tag{A 1}$$

where

$$\mathsf{L} = \begin{pmatrix} \nabla^4 & Ra\nabla_1^2 & 0 \\ 1 & \nabla^2 & 0 \\ \partial_{zz}|_1 & 0 & -M^{(0)}\nabla_1^2 \end{pmatrix}, \quad \boldsymbol{U} = \begin{pmatrix} w^{(1)} \\ \theta^{(1)} \\ \theta_1^{(1)} \end{pmatrix}. \tag{A 2}$$

The boundary condition involving the eigenvalues $M^{(0)}$ has been included in the operator L. The remaining boundary conditions are

$$w^{(1)} = \partial_z w^{(1)} = \theta^{(1)} = 0 \quad \text{at} \quad z = 0, \tag{A 3}$$

$$w^{(1)} = \partial_z \theta^{(1)} + h\theta^{(1)} = 0 \quad \text{at} \quad z = 1. \tag{A 4}$$

The operator L^* adjoint to L is defined by

$$\langle \boldsymbol{U}^*, \mathsf{L}\boldsymbol{U} \rangle = \langle \boldsymbol{U}, \mathsf{L}^*\boldsymbol{U}^* \rangle, \tag{A 5}$$

where $\boldsymbol{U}^*[w^*, \theta^*, \partial_z w^*|_1]$ is the adjoint eigenvector, the solution of

$$\mathsf{L}^*\boldsymbol{U}^* = 0. \tag{A 6}$$

By integration by parts of the left-hand side of (A 5) and use of (A 3) and (A 4), one obtains

$$\mathbf{L}^* = \begin{pmatrix} \nabla^4 & 1 & 0 \\ Ra\nabla_1^2 & \nabla^2 & 0 \\ 0 & -(\partial_z + h)_1 & -M^{(0)}\partial_z \nabla_1^2|_1 \end{pmatrix}, \tag{A 7}$$

with the corresponding adjoint boundary conditions

$$w^* = \partial_z w^* = \theta^* = 0 \quad \text{at} \quad z = 0, \tag{A 8}$$

$$w^* = \partial_{zz} w^* = 0 \quad \text{at} \quad z = 1. \tag{A 9}$$

In analogy with the linear problem set up in §3, one expresses the solution of (A 2) in the form

$$w^* = W^*(z)\,\phi^+(x, y), \tag{A 10}$$

$$\theta^* = \Theta^*(z)\,\phi^+(x, y), \tag{A 11}$$

where ϕ^+ has been defined by (4.7)

After substitution of (A 10) and (A 11) in (A 6), one obtains the equations governing the behaviour of the amplitude W^* and Θ^*, namely

$$(\mathrm{D}^2 - k^2)^2 W^{2*} + \Theta^* = 0, \tag{A 12}$$

$$(\mathrm{D}^2 - k^2)\,\Theta^* - Ra\,k^2 W^* = 0, \tag{A 13}$$

with the boundary conditions

$$W^* = \mathrm{D}W^* = \Theta^* = 0 \quad \text{at} \quad z = 0, \tag{A 14}$$

$$W^* = \mathrm{D}^2 W^* = \mathrm{D}\Theta^* + h\Theta^* - M^{(0)}k^2 DW^* \quad \text{at} \quad z = 1. \tag{A 15}$$

Equations (A 12) and (A 13) can be obtained as Euler–Lagrange equations of the variational principle

$$\delta \int_0^1 \left\{ \mathrm{D}^2 W^* - k^2 W^*)^2 + \frac{1}{Ra\,k^2}[(D\Theta^*)^2 + k^2\Theta^{*2}] + 2\Theta^* W^* \right\} \mathrm{d}z - \delta\left(\frac{1}{Ra}\right)\left[2M^{(0)}\Theta^* \mathrm{D}\overset{0}{W}{}^* - \frac{h}{k^2}\Theta^{*2} \right]_1 = 0. \tag{A 16}$$

The boundary conditions

$$\mathrm{D}^2 W^* = 0 \quad \text{at} \quad z = 0, \quad \mathrm{D}^2 W^* = \mathrm{D}\Theta^* + h\theta^* - M^{(0)}k^2 \mathrm{D}W^* = 0 \quad \text{at} \quad z = 1 \tag{A 17}$$

appear as natural conditions of the variational equation (A 16). The zero above $\mathrm{D}W^*$ means that the corresponding quantity must be frozen during the variational procedure. This is the reason why the variational principle (A 16) is not an 'exact' one but must be classified as a 'restricted' variational principle (Finlayson 1972; Lebon 1981). Despite this restricted character, one is allowed to use the classical variational methods, like the Rayleigh–Ritz technique.

A.2. *The adjoint problem of the perturbed problem*

The adjoint solution of the perturbed problem is similar to that presented in §A.1: it suffices to put a tilde on each quantity. Slight modifications arise when the perturbed wavenumber $\tilde{\boldsymbol{k}}$ differs from the reference wavenumber $\boldsymbol{k}$. In this case $\sigma^{(0)}$

is not zero and the problem must be reconsidered. Instead of (A 2), the linear operator is then

$$\tilde{\mathsf{L}} = \begin{pmatrix} \nabla^4 - P^{-1}\sigma^{(0)}\nabla^2 & Ra\nabla_1^2 & 0 \\ 1 & \nabla^2 - \sigma^{(0)} & 0 \\ \partial_{zz}^2|_1 & 0 & -M^{(0)}\nabla_1^2 \end{pmatrix},$$

and it is found that the adjoint operator

$$\tilde{\mathsf{L}}^* = \begin{pmatrix} \nabla^4 - P^{-1}\sigma^{(0)}\nabla^2 & 1 & 0 \\ Ra\,\nabla_1^2 & \nabla^2 - \sigma^{(0)} & 0 \\ 0 & -(\partial_z + h)_1 & -M^{(0)}\partial_z\nabla_1^2 \end{pmatrix},$$

with the adjoint boundary conditions

$$\tilde{w}^* = \partial_z\tilde{w}^* = \tilde{\Theta}^* = 0 \quad \text{at} \quad z = 0,$$

$$\tilde{w}^* = \partial_{zz}\tilde{w}^* = 0 \quad \text{at} \quad z = 1.$$

REFERENCES

Bénard, H. 1900 *Rev. Gén. Sci. Pure Appl.* **11**, 1261.

Block, M. 1956 *Nature* **178**, 650.

Busse, F. 1967 *J. Maths & Phys.* **46**, 140.

Busse, F. 1978 *Rep. Prog. Phys.* **41**, 1929.

Chandrasekhar, S. 1961 *Hydrodynamic and Hydromagnetic Stability*. Clarendon.

Cloot, A. 1983 Ph.D. thesis, Liège University.

Davis, S. H. 1969 *J. Fluid Mech.* **39**, 347.

Davis, S. H. & Homsy, G. 1980 *J. Fluid Mech.* **98**, 527.

E.S.A. 1981 Microgravity research in space. *European Space Agency Rep.* BR-05.

Finlayson, B. 1972 *The Method of Weighted Residuals and Variational Principles*. Academic.

Friedman, B. 1956 *Principles and Techniques of Applied Mathematics*. Wiley.

Gorkov, L. 1957 *Sov. Phys. JETP* **6**, 311.

Joseph, D. D. 1966 *Arch. Rat. Mech. Anal.* **22**, 163.

Koschmieder, E. 1981 In *Proc. Euromech Coll. 138, Karlsruhe, March 1981*, pp. 29–34, Verlag 6. Braun.

Kraska, J. & Sani, R. 1979 *Intl J. Heat Mass Transfer* **22**, 535.

Lebon, G. 1980 In *Recent Developments in Thermomechanics*; *CISM Courses*, vol. 262, pp. 221–412 (ed. G. Lebon & P. Perzyna). Springer.

Lebon, G. 1982 In *Stability of Thermodynamic Systems*, pp. 41–93 (ed. J. Casas-Vazquez & G. Lebon). Lecture Notes in Physics, vol. 164. Springer.

Lebon, G. & Cloot, A. 1982 *Acta Mech.* **43**, 141.

Lebon, G. & Perez-Garcia, C. 1980 *Bull. Acad. R. Belg.* **66**, 520.

Malkus, W. & Veronis, G. 1958 *J. Fluid Mech.* **4**, 225.

Nield, D. 1964 *J. Fluid Mech.* **19**, 341.

Palm, E. 1975 *Ann. Rev. Fluid Mech.* **7**, 30.

Pearson, J. R. A. 1958 *J. Fluid Mech.* **4**, 489.

Rosenblat, S., Davis, S. H. & Homsy, G. 1982 *J. Fluid Mech.* **120**, 91.

Scanlon, J. & Segel, L. 1967 *J. Fluid Mech.* **30**, 149.

Schlüter, A., Lortz, D. & Busse, F. 1965 *J. Fluid Mech.* **23**, 129.

Scriven, L. & Sternling, C. 1964 *J. Fluid Mech.* **21**, 321.

Serrin, J. 1959 *J. Fluid Mech.* **3**, 1.

Smith, K. A. 1966 *J. Fluid Mech.* **24**, 401.

Stuart, J. 1960 *J. Fluid Mech.* **9**, 353.

Vidal, A. & Acrivos, A. 1966 *Phys. Fluids* **9**, 615.